Legend and presentation points:
- Scientific relevance of Hafnia-based ferroelectrics;
- Targeted application, motivation and constraints;
- Fabrication process and parameters for optimization;
- Analysis based on insights from MICRO-621 course;
- Comparison with current state of the art fabrication.

ACS APPLIED ELECTRONIC MATERIALS

pubs.acs.org/acsaelm Article

# Sputtered Ferroelectric Hafnium−Zirconium Oxide with High Remanent Polarization after Back-End-of-Line Compatible Annealing

Xuetao Wang,* Thomas Mikolajick, and Matthias Grube*

Cite This: *ACS Appl. Electron. Mater.* 2022, 4, 6142−6148 Read Online

ACCESS | Metrics & More | Article Recommendations | Supporting Information

**ABSTRACT:** The back-end-of-line (BEOL) processing compatibility of sputtered ferroelectric hafnium zirconium oxide (HZO) thin films is demonstrated on sputtered TiN/HZO/TiN thin-film ferroelectric capacitors. This promises an easy integration of $HfO_2$-based ferroelectrics for applications such as non-volatile memories. It is found that the sputtering pressure can significantly influence the film growth and morphology of HZO layers. At a sputtering pressure of $5 \times 10^{-3}$ mbar, deposited HZO films show high remanent polarization ($P_r$) after 400 °C annealing, indicating a high fraction of the polar orthorhombic crystal structure. Additionally, the ferroelectric properties of HZO films were improved by proper tuning of sputtering power. We are able to show that a BEOL-compatible thermal budget (at 400 °C for 1 h) is enough to provoke good ferroelectricity with the $2P_r$ of up to 36 $\mu C/cm^2$ and an endurance of up to $10^7$ cycles in sputtered HZO films. With such modifications, the sputtered HZO films become comparable to atomic-layer deposited HZO films with a similar thermal budget.

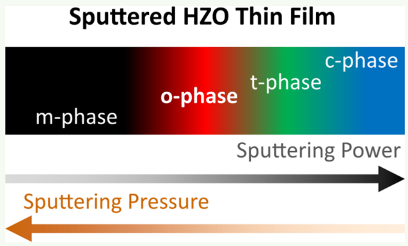


**KEYWORDS:** *ferroelectric, hafnium zirconium oxide, sputtering, back-end-of-line, process pressure*

## 1. INTRODUCTION

Hafnia-based ferroelectrics (FEs), as a feasible replacement for conventional perovskite FEs in non-volatile memory (NVM) applications, provide better scalability and compatibility with complementary metal-oxide-semiconductor (CMOS) processes.[1] Currently, one of the mainstream FE memory elements is the FE random access memory (FeRAM).[1,2] FeRAM is a non-volatile variation of dynamic RAM, whose dielectric capacitor is replaced by an FE capacitor (FeCap).[2] With the help of the non-volatile property of the FE layer, the information can be retained in FeRAM without power supply, reducing the energy consumption in most application scenarios.[3] In order to avoid significant changes in the CMOS processes, FeCaps can be integrated into back-end-of-line (BEOL) processes. The BEOL integration comes with the price of some additional restrictions. One of the most severe restrictions is the maximum temperature for crystallization that should equal 400 °C or below.[1,4,5] Therefore, a low crystallization temperature below 400 °C of $HfO_2$-based FEs is needed. With the help of atomic layer deposition (ALD) processes, zirconium-doped hafnia (HZO) system can meet this requirement, enabling the BEOL integration of $HfO_2$-based FeCaps.[6−8] Moreover, the HZO system exhibits outstanding FE properties and a broad process window, which relaxes the process restraint.[9,10]

as well as FeFET and FTJ

explain motivation for BEOL

While ALD is dominating the commercial market of fabricating $HfO_2$-based thin film systems, sputtering joins the competition with a number of advantages: stabilization of the FE crystal phase favored by the non-equilibrium process, high throughput due to a high deposition rate, room-temperature deposition instead of 250−300 °C during ALD, and the absence of carbon contamination from ALD precursor residuals.[11−13] Due to the energetic bombardment during the deposition and the non-compatibility to 3-dimensional (3D) processing, sputtering is not preferred in any interface-sensitive and 3D structures like gate stack front-end-of-line processes, while for BEOL integration processes, sputtering could be an excellent alternative to ALD and improve the throughput. However, the previous work on sputtered $HfO_2$-based FE indicates that either temperatures significantly above 450 °C were necessary to activate the FE property or the FE response is relatively weak with BEOL-compatible thermal treatments.[14,15] Therefore, the BEOL compatibility of sputtered $HfO_2$-based FE needs to be improved to reach the requirements for NVM applications.

motivation for sputtering

sputtering deposition is application specific

In this work, a significant leap forward in the BEOL compatibility of sputtered HZO capacitors is achieved by tuning the sputtering parameter to enhance the FE property and simultaneously lower the thermal crystallization budget of 10 nm thin HZO films. An enhanced FE crystal phase fraction

**Received:** September 19, 2022
**Accepted:** November 15, 2022
**Published:** November 23, 2022

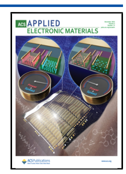

Main goal: optimize ferroelectric response, i.e. formation of polar othorhombic phase, and endurance with thermal constraints on annealing







https://doi.org/10.1021/acsaelm.2c01259
*ACS Appl. Electron. Mater.* 2022, 4, 6142−6148

HfO2 has different phases with different thermodynamic internal energies at which they can be stabilized. The transition from low to high energy phase generally follows the sequence: monoclinic (m), orthorhombic (o), tetragonal (t) and cubic (c). To stabilize the metastable polar o-phase (the one that exhibits ferroelectricity) doping and/or strain engineering are necessary, as well as accurate tuning of the growth conditions.

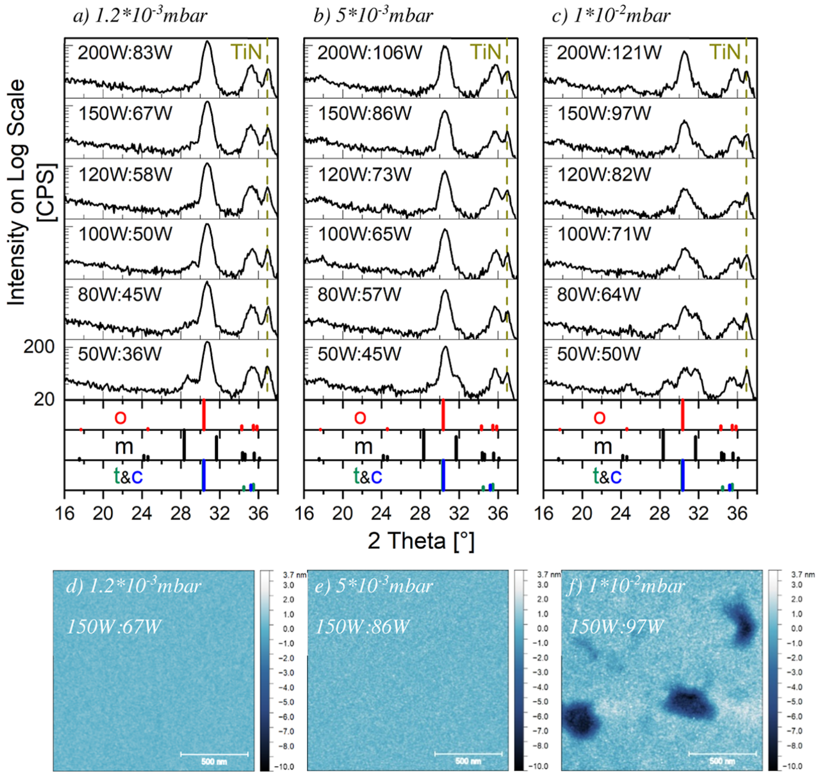


**Figure 1.** GIXRD patterns and AFM images of sputtered HZO (87:13) with different sputtering pressures and powers in an FeCap stack after 800 °C annealing. The bar charts of (a−c) represent the different $HfO_2$ crystal phases retrieved from the ICCD database.[17] Since the *y*-axis scale (intensity) is the same for all GIXRD patterns, it is only shown once in (a). The abbreviation "*xx* W:*yy* W" indicates the used powers for the $HfO_2$ and $ZrO_2$ target, respectively. HZO processed at (a) $1.2 \times 10^{-3}$, (b) $5 \times 10^{-3}$, and (c) $1 \times 10^{-2}$ mbar. HZO processed with (d) 150 W:67 W at $1.2 \times 10^{-3}$ mbar (TiN top electrode etched), (e) 150 W:86 W at $5 \times 10^{-3}$ mbar (TiN top electrode etched), and (f) 150 W:97 W at $1 \times 10^{-2}$ mbar (TiN top electrode etched).

can be formed during BEOL-compatible annealing (400 °C, 1 h) using an optimized sputtering pressure. The FE polarization is further improved by manipulating the sputtering power. In particular, the remanent polarization ($P_r$) of the sputtered HZO satisfies the FeRAM application goal defined by the International Roadmap for Devices and Systems 2021 (IRDS2021).[16]

Technology benchmark

## 2. EXPERIMENTAL METHODS

An ultra-high-vacuum sputter cluster (Bestec GmbH) was used to deposit the whole FeCap on a p-type Si substrate with the stack made of a 10 nm thick TiN bottom electrode, a 10 nm thick HZO FE layer, and a 25 nm thick TiN top electrode. The sputtering targets for TiN and HZO films are all 3 inches. TiN films were prepared by DC sputtering (150 W) from a Ti target at $1.2 \times 10^{-3}$ mbar with the process gases Ar (20 sccm) and $N_2$ (4 sccm). For HZO films, simultaneous RF sputtering of a $HfO_2$ and a $ZrO_2$ target in a confocal arrangement was implemented. The sputtering pressure for HZO ranged from $1.2 \times 10^{-3}$ to $1 \times 10^{-2}$ mbar with a process gas flow of 20 sccm Ar. A constant $ZrO_2$ concentration in HZO was regulated by varying the sputtering power of the $ZrO_2$ (36−121 W) and $HfO_2$ (50−200 W) targets. After deposition, the FeCaps were annealed in an $N_2$ atmosphere to crystallize the HZO films using a rapid thermal processing tool (SHS2800, AST Elektronik GmbH). The annealing temperature is measured using the built-in pyrometer, which has been calibrated by using a thermocouple wafer. Finally, Ti (5 nm)/Pt (40 nm) metal dots were deposited on top using an evaporator (Bestec GmbH), and the top electrodes of the FeCaps were isolated by a wet chemical etching with a solution of 30% $NH_4OH$/30% $H_2O_2/H_2O$ = 1:2:50.

The crystal structure was characterized by grazing incident X-ray diffraction (GIXRD) with a Cu X-ray source (D8 Discover, Bruker Corporation). The crystal phase references used were taken from ICCD PDF cards, including 04-003-6960 orthorhombic (o)-phase $HfO_2$, 00-034-0104 monoclinic (m)-phase $HfO_2$, 04-011-8820 tetragonal (t)-phase $HfO_2$, 00-053-0560 cubic (c)-phase $HfO_2$, and 00-038-1420 c-phase TiN.[17] Atomic force microscopy (AFM) was used to investigate the surface morphology of HZO in the FeCap stacks (Dimension 3100, Bruker Corporation). The FE properties were analyzed using a TF Analyzer 3000 (aixACCT Systems), including polarization−voltage (*PV*) and current−voltage (*IV*) characteristics measured at 3 V and 1 kHz and endurance measurements performed at 3 V and 10 kHz.

## 3. RESULTS AND DISCUSSION

The optimal $ZrO_2$ concentration to reach the highest $P_r$ was found to be about 13% $ZrO_2$ in sputtered HZO thin films,[13,15] which is lower compared to the optimal concentration in ALD-deposited HZO of about 50% $ZrO_2$.[18] This discrepancy could be caused by the energetic bombardment and easy generation of oxygen vacancies during sputtering.[11,13,15] Therefore, HZO films with 13% $ZrO_2$ content were deposited as a FE layer, and these films will be denoted as HZO (87:13) in the following. Different values for the sputtering pressure and the sputtering power were employed for the deposition, exploring the effect of these parameters on the film growth of the HZO layers. The influence of the sputtering power on pure $HfO_2$ and $Hf_{0.5}Zr_{0.5}O_2$ was investigated in the previous work.[15,19] These studies suggest that increasing the sputtering power favors high-symmetry phases (o-, t-, and c-phases) after annealing,

Optimization space, 3 parameters: sputtering pressure, sputtering power and annealing temperature


https://doi.org/10.1021/acsaelm.2c01259
ACS Appl. Electron. Mater. 2022, 4, 6142−6148

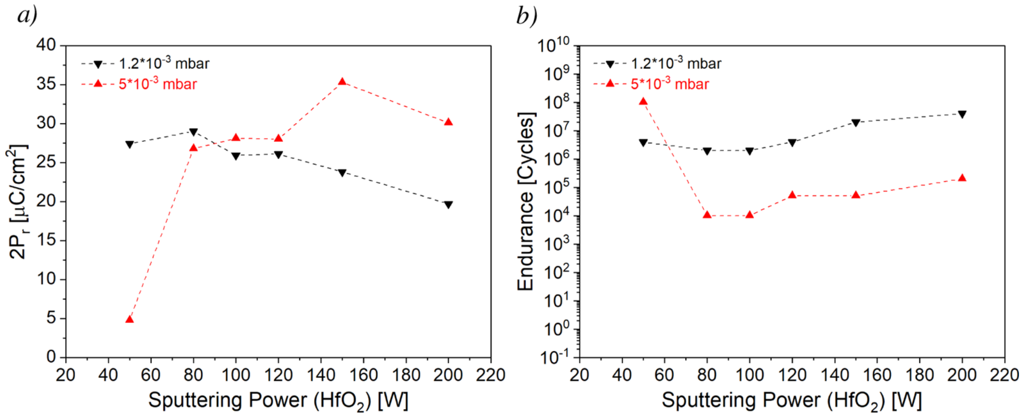


**Figure 2.** FE properties of the FeCaps annealed at 800 °C as a function of the sputtering power for the HZO (87:13). FeCaps with HZO processed at $1.2 \times 10^{-3}$ and $5 \times 10^{-3}$ mbar: (a) $2P_r$ after wake-up and (b) endurance. The connection lines are used for guiding the trend.

while reduced power favors the low-symmetry phase (m-phase) after annealing. This power-induced phase transition was verified on HZO (87:13) films in this study. Before annealing, the as-deposited HZO (87:13) films were still amorphous, and hence, their GIXRD results are not shown here. Figure 1 compares the crystal structure and surface morphology of HZO (87:13) films annealed at 800 °C. For a simple naming of the films, the sputtering powers for both targets in HZO film are abbreviated, for instance, as 200 W:83 W. Here, the first number is the sputtering power for the $HfO_2$ target, while the second number is the one for the $ZrO_2$ target. (notation) Figure S1 reveals the linear correlation between deposition rate of the HZO (87:13) films and the sputtering power at the targets. Moreover, the deposition rate decreases with the sputtering pressure. Due to the different atomic mass and binding energy of $HfO_2$ and $ZrO_2$, the deposition rate of both oxides is different at the same applied power. Additionally, the deposition rates of $HfO_2$ and $ZrO_2$ exhibit a different dependency on the process pressure. In order to retain 13% $ZrO_2$ in the HZO films, the total sputtering power of the two targets has to be slightly modified under varying pressure. However, the sputtering power of the $HfO_2$ target was kept constant, preserving similar process conditions for different sputtering pressures. X-ray photoelectron spectroscopy confirms the stoichiometry of HZO (87:13) on the selected samples (Table S1).

Comparing the GIXRD results of samples with different sputtering powers at a process pressure of $1.2 \times 10^{-3}$ mbar (Figure 1a), the high-symmetry phases dominate the crystal structure for all HZO films after annealing. The sample with 50 W:36 W shows an enhanced reflection intensity for m-phase at 28.3° $2\theta$ and a sharper reflection peak compared to the samples with increased sputtering power. At a sputtering pressure of $5 \times 10^{-3}$ mbar (see Figure 1b), the crystal structure transformation of HZO (87:13) films still follows the same trend as the films do at $1.2 \times 10^{-3}$ mbar. However, the crystal texture changed. Significantly, the sample deposited at a low power (50 W:45 W) shows an enhanced 111 reflection of the m-phase at 31.6° $2\theta$. In contrast, the −111 reflection of the m-phase at 28.3° is more substantial for the sample deposited at a lower pressure of $1.2 \times 10^{-3}$ mbar and with a similar power. Additionally, two weak reflections appeared at $2\theta$ of 17.7 and 24.6° for $5 \times 10^{-3}$ mbar samples, which can be attributed to the o- or m-phase of HZO. The reflections are 001 for the m-phase and 100 for the o-phase at 17.7° $2\theta$, and at 24.6°, the reflections are 110 and 011 for the m-phase and 110 for the o-phase.[17] A more notable phase change happened at a pressure of $1 \times 10^{-2}$ mbar (Figure 1c). The high-symmetry phases are the main crystal phases in the HZO film at high sputtering powers, but the m-phase starts to take up a substantial amount of the crystal phase fraction at medium and low powers. This sputtering pressure-induced phase transformation can be explained by the change of the mean free path and the kinetic energy of the sputtered species, which were altered by the sputtering pressure. At a lower sputtering pressure, the vapor and plasma density are low, leading to a low amount of collisions between particles. Therefore, sputtered species have a longer mean free path and higher kinetic energy. When sputtered atoms and molecules arrive at the substrate, they have excessive energy to diffuse to the position which prefers lowering the overall free energy of the system.[20,21] After diffusion, the interaction between adsorbed species is smaller than their bonds to the substrate, which leads to two-dimensional growth. The nuclei have a large surface area, facilitating the formation of the high-symmetry phases (e.g., o-, t-, and c-phases).[22−24] Increasing sputtering pressure increases the collisions in the vapor phase, reducing the sputtered particles' mean free path and kinetic energy. Since the mobility of the sputtered atoms and molecules is reduced, adsorbed species are inclined to coalesce instead of diffusing to other spots.[20,21] Moreover, due to the more frequent collisions in the vapor phase, more clusters instead of single atoms and molecules form and arrive at the substrate. These two effects could stimulate the interaction between adsorbed species and initiate the island growth mode on the substrate.[23,24] The islands contain agglomerated nuclei whose surface-to-volume ratio is small, promoting the thermodynamically stable bulk phase (e.g., m-phase) after annealing.[22] Sputtering pressure and power affect the films' crystal growth in opposite directions. Thus, one parameter could be used to compensate for the influence of the other. For instance, a high sputtering power could generate more oxygen vacancies in the film and suppress the m-phase formation, which would otherwise be favored at high sputtering pressure. Therefore, in order to reach the optimal polar o-phase fraction, the sputtering power and pressure need to be tuned simultaneously.

The AFM images (Figure 1d−f) disclose the growth and surface morphology evolution of HZO films at different sputtering pressures. A couple of steps were performed before the AFM measurements to ensure the same processing


https://doi.org/10.1021/acsaelm.2c01259
ACS Appl. Electron. Mater. 2022, 4, 6142−6148

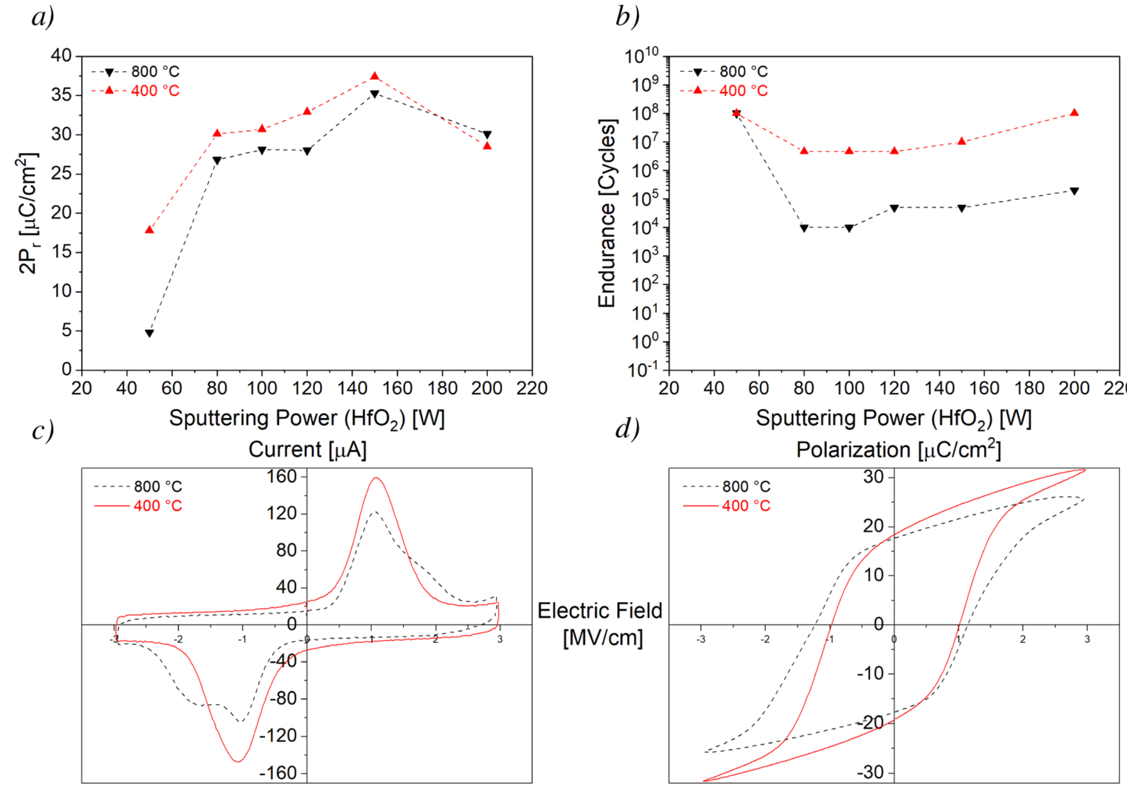


Important point: Anneling favours the phase transition. The amount of t-phase after sputtering has to be balanced to the energy provided by the annealing, so to have enough to transition to o-phase, while not leaving any t-phase untransitioned.

**Figure 3.** FE properties of the FeCaps with HZO (87:13) processed at $5 \times 10^{-3}$ mbar. FeCaps annealed at 800 and 400 °C: (a) $2P_r$ (after wake-up) as a function of the sputtering power; (b) endurance as a function of the sputtering power; (c) *IV* curves for HZO (87:13) sputtered at 150 W:86 W; (d) *PV* curves for HZO (87:13) sputtered at 150 W:86 W. The connection lines are used for guiding the trend.

High pressure results in non-uniform deposition: this is due to a reduction of the mean free path of sputtered atoms, that results in lower kinetic energy, lower diffusion at the substrate and more clustering. In addition, higher pressure results in a lower target ejection rate and deposi -tion rate. The higher pressure process is exluded.

condition. The as-deposited FeCap stacks were annealed at 800 °C. Afterward, the TiN top electrodes were etched away, exposing the HZO films to the surface. It can be seen that the surface is smooth, and the average grain sizes are in the range of several nanometers for samples sputtered at $1.2 \times 10^{-3}$ and $5 \times 10^{-3}$ mbar. On the other hand, some voids having a depth down to 10 nm can be spotted in samples sputtered with a pressure of $1 \times 10^{-2}$ mbar. The height profiles along the horizontal line were extracted to demonstrate the topography of the HZO films (Figure S2). The surface morphology matches the film growth mode for HZO films sputtered at a different pressure. At $1.2 \times 10^{-3}$ mbar, atoms and molecules tend to diffuse to the position which can minimize the average free energy of the film. As a result, the defects are filled. This will help to form a compact and dense layer exhibiting layer-by-layer growth. The surface roughness remained similar with increasing pressure from $1.2 \times 10^{-3}$ to $5 \times 10^{-3}$ mbar, indicating no significant variation of the grain size. At an elevated pressure of $1 \times 10^{-2}$ mbar, atoms and molecules have lower energy to diffuse and thus merge to form islands, resulting in the formation of voids.

Analysis for 800°C annealing

Figure 2 displays the $2P_r$ and the endurance of a sample annealed at 800 °C as a function of the applied sputter power for two different sputtering pressures. As discussed previously, the overall sputtering power for $HfO_2$ and $ZrO_2$ targets was not the same for different pressures if a constant concentration is targeted. Hence, the sputtering power for $HfO_2$ is used to represent the samples with varying sputter power in the plot. Figure 2a shows that $2P_r$ changes with sputtering power and pressure. For both sputtering pressures, $2P_r$ first increases and later drops with increasing sputtering power, which is consistent with previous work for pure $HfO_2$.[15] This dependence on the sputtering power is already seen in the GIXRD results, showing the crystal phase transforming from the m-phase to the t-/c-phases by increasing the sputtering power. Tuning the sputtering power to a medium value boosts the polar o-phase fraction. It is worth noting that the maximum $2P_r$ could be enhanced by elevating the sputtering pressure from $1.2 \times 10^{-3}$ to $5 \times 10^{-3}$ mbar, except for the samples with a low power (50 and 80 W for $HfO_2$). The low $2P_r$ value especially seen in the sample with 50 W $HfO_2$ power can be explained by a high m-phase fraction with only a minor polar o-phase content. Moreover, the optimal sputtering power was shifted from 80 W for $HfO_2$ to 150 W for $HfO_2$ when increasing the process pressure from $1.2 \times 10^{-3}$ to $5 \times 10^{-3}$ mbar. The optimal power shift matches the crystal structure evolution of the HZO films. After increasing the sputtering pressure, more t- and c-phases transformed into o- or m-phase during annealing, which is supported by the GIXRD results and enhanced $2P_r$ value. In comparison, a high sputtering power could counter this effect and transit the crystal phases into the metastable polar o-phase instead of the non-polar m-phase. Although $2P_r$ was improved, the endurance of the FeCap was reduced at a higher sputtering pressure as shown in Figure 2b. The samples, which were processed at $1 \times 10^{-2}$ mbar, exhibited a considerable leakage contribution and in some cases even shorts. Hence, they are not presented here. The apparent voids in the HZO film revealed by Figure 1f could explain this result. In this case, the TiN top electrode film could fill those voids and contact the TiN bottom electrode, shorting the stack.

In addition to the deposition process parameters, the thermal budget can also influence the crystal structure of $HfO_2$-based films.[25] The crystal phase of the $HfO_2$-based



https://doi.org/10.1021/acsaelm.2c01259
ACS Appl. Electron. Mater. 2022, 4, 6142−6148

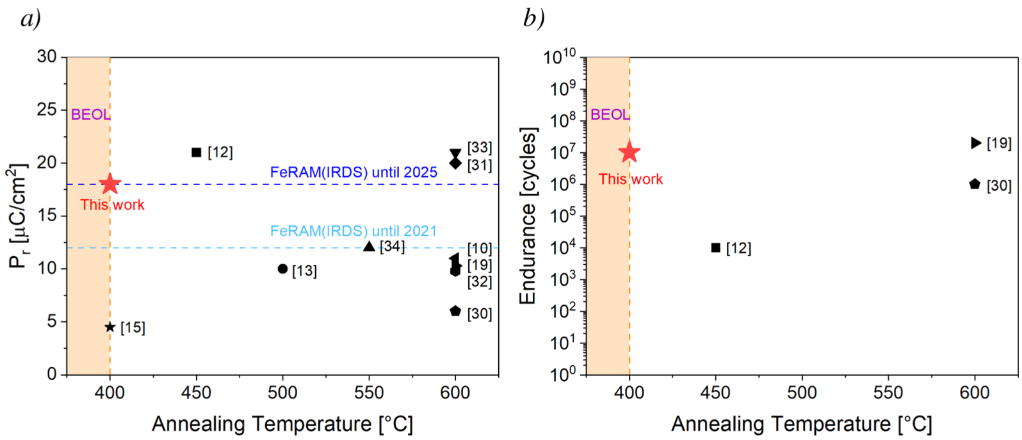


**Figure 4.** Comparison of FE properties of fully sputtered FeCaps from data in refs 10 12 13 15 19 30,−34 and this work, including the IRDS[2021] guideline.[16] The annealing temperature range of BEOL processes is highlighted by an orange area: (a) $P_r$ (after wake-up) of the samples annealed at different temperatures; (b) endurance of the samples annealed at different temperatures.

system during the thermal treatment usually develops from amorphous into the crystalline t-phase and later to o-phase and m-phase.[25−27] Sufficient thermal energy could help the HZO film to overcome the energy barrier for transformation from the t-phase to the o-phase. In the meanwhile, excessive energy could enhance the transition from the t-phase to the m-phase.[25−27] After annealing at 800 °C, the samples processed at $5 \times 10^{-3}$ mbar showed higher $2P_r$, which suggests a higher polar o-phase fraction. Nevertheless, these samples suffered from lower endurance. This "$P_r$-endurance dilemma" is consistently present in previous work, which can be caused by the fact that higher $P_r$ induces higher electric fields and more charges are injected into the film.[28] Consequently, electric field cycling could trap more charges, pin more domains, create more defects within the film, and eventually lead to the electric breakdown. High-temperature annealing could further worsen the situation by promoting charge trapping, domain pinning, undesired phase (e.g., m-phase), and defects (e.g., oxygen vacancies).[11,29] Therefore, lowering the annealing temperature on the HZO processed at $5 \times 10^{-3}$ mbar could even be beneficial to improve the reliability. Meanwhile, our previous work implies that low-power sputtered HZO films could crystallize and exhibit ferroelectricity even after 1 h annealing at 400 °C (BEOL-compatible annealing).[15] Additionally, high pressure has a similar effect to low power, lowering the crystallization temperature of sputtered HZO, as demonstrated in structural and electric results.[15] Consequently, BEOL-compatible annealing might also be beneficial to HZO films that were fabricated at a higher sputtering pressure. As shown in Figure S3, the GIXRD results of the $5 \times 10^{-3}$ mbar samples prove that BEOL-compatible annealing could crystallize the HZO films regardless of the sputtering power. Compared to the samples annealed at 800 °C, the 400 °C annealed samples show no distinct difference in the diffraction patterns. Nonetheless, the conclusion that two annealing temperatures provide the same HZO crystal quality cannot be drawn based on this observation. Figure S3 displays that the HZO o-, t-, and c-phase reflections are very close to each other at 30.5° 2$\theta$, and it is challenging to resolve individual contributions from each phase. Thus, electrical measurements are necessary to unravel the subtle microstructural change with different annealing temperatures.

In addition, a high T annealing can favour defects and charge trapping into the ferroelectric layer.

Figure 3 compares the $2P_r$, the endurance, and selected hysteresis curves of HZO samples annealed at 800 and 400 °C, which were deposited at $5 \times 10^{-3}$ mbar. It is evident from Figure 3a that decreasing the annealing temperature from 800 to 400 °C improves the $2P_r$ value for most of the samples. Especially, the sample with 50 W for $HfO_2$ shows a substantial increase of the $2P_r$ from ca. 5 to ca. 18 $\mu C/cm^2$ by lowering the annealing temperature to 400 °C. This progress proves the previous assumption that 800 °C delivered excessive energy to the HZO films deposited at $5 \times 10^{-3}$ mbar. For samples deposited with a low sputtering power, the t-phase transformed into the non-polar o-phase and m-phase during 800 °C annealing. However, for high-power sputtered samples, more defects and harmful diffusion were initiated during 800 °C annealing. Using a lower annealing temperature, a higher polar o-phase fraction could be formed, and defects and detrimental diffusion could be suppressed. Figure 3b shows that the endurance of the FeCaps is improved by 2−3 orders of magnitude after a lower-temperature annealing, indicating that 400 °C, 1 h is a proper thermal budget. How the $P_r$ evolves with the electric field cycling for the samples annealed at 400 °C is displayed in Figure S4. A typical $HfO_2$-based FE cycling behavior can be witnessed, which comprises wake-up, plateau, fatigue, and breakdown. According to Figure 3c,d, the sample annealed at 400 °C shows less leakage contribution, more homogeneous switching, and a lower coercive field. This confirms that an extra thermal budget would induce undesired phase transitions, diffusion, and defects. Most importantly, with BEOL-compatible annealing, sputtered HZO can provide good FE properties with the highest $2P_r$ of 36 $\mu C/cm^2$ and an endurance of up to $10^7$ cycles if the sputtering parameters are well chosen.

A summary of previous studies on sputtered HZO[10,12,13,15,19,30−34] and this work is visualized in Figure 4. Most of the published results show that an annealing temperature higher than 500 °C was required to achieve good FE properties of the sputtered HZO films. Our previous work showed that BEOL-compatible annealing was sufficient to provoke FE properties of sputtered HZO films.[15] However, the $P_r$ value was too low for the application in FeRAM. Meanwhile, more than half of the reported $P_r$ values did not reach 12 $\mu C/cm^2$, which is the target for FeRAM application until 2021 by the IRDS[2021].[16] The sputtered HZO films processed in this study meet the required $P_r$ of 18 $\mu C/cm^2$ defined as a target for FeRAM application until 2025 by the IRDS[2021].[16] In addition to the $P_r$, reliability, such as endurance,

To this compari-son on sputtered HZO, we will add a reference to state of the art ALD deposited HZO. ALD is the current technique used in Nanolab for the deposition of doped HfO2.



https://doi.org/10.1021/acsaelm.2c01259
ACS Appl. Electron. Mater. 2022, 4, 6142−6148

is also an important parameter for the FeRAM application. In this work, the sample survived until $10^7$ cycles under the electric field stress, which is in line with the reported value.[19,30] It was recently shown that scaling the capacitor area to more realistic values compared to the large test capacitors used in this study will further increase the endurance.[35]

## 4. CONCLUSIONS

In conclusion, we have demonstrated the BEOL processing compatibility of the sputtered HZO-based FeCap. The sputtering pressure is essential to modify the crystallization temperature of the polar o-phase of HZO. After BEOL-compatible annealing of 400 °C for 1 h and electric wake-up, the sputtered HZO FeCap could exhibit a $2P_r$ of 36 $\mu C/cm^2$ and an endurance of up to $10^7$ cycles. In this work, the FE properties of the sputtered HZO samples approach the FE properties of ALD-deposited HZO samples of a similar thickness with a 400 °C annealing, which was reported to have the $2P_r$ and endurance of about 40 $\mu C/cm^2$ and $10^7$ to $10^8$ cycles, respectively.[36] Since sputtering is a non-equilibrium process and sputtered HZO has not been studied as much as ALD-deposited HZO, one could expect that sputtered HZO FeCaps have the potential to reach the same FE properties as ALD-deposited HZO FeCaps. In addition, the higher throughput makes sputtering an excellent alternative technique to ALD to fabricate HZO-based FeCaps in BEOL processes.

## ASSOCIATED CONTENT

### Supporting Information

The Supporting Information is available free of charge at https://pubs.acs.org/doi/10.1021/acsaelm.2c01259.

Deposition rate of the HZO films, surface chemical composition of the HZO samples by X-ray photoelectron spectroscopy, AFM height profiles along the horizontal line of the samples, GIXRD of the $5 \times 10^{-3}$ mbar samples, and endurance measurement of the $5 \times 10^{-3}$ mbar samples (PDF)

## AUTHOR INFORMATION

### Corresponding Authors

**Xuetao Wang** − *NaMLab gGmbH, Dresden 01187, Germany*; orcid.org/0000-0002-0529-8817; Phone: +49-351-2124990-22; Email: Xuetao.Wang@namlab.com

**Matthias Grube** − *NaMLab gGmbH, Dresden 01187, Germany*; Phone: +49-351-2124990-28; Email: Matthias.Grube@namlab.com

### Author

**Thomas Mikolajick** − *NaMLab gGmbH, Dresden 01187, Germany; Chair of Nanoelectronics, TU Dresden, Dresden 01187, Germany*; orcid.org/0000-0003-3814-0378

Complete contact information is available at: https://pubs.acs.org/10.1021/acsaelm.2c01259

### Author Contributions

The manuscript was written through contributions of all authors. All authors have given approval to the final version of the manuscript.

### Funding

X.W, M.G., and T.M. were financially supported out of the Saxonian State budget approved by the delegates of the Saxon State Parliament. This work was financially supported by the European Fund for Regional Development EFRD, Europe supports Saxony, and by funds released by the delegates of the Saxon State Parliament.

### Notes

The authors declare no competing financial interest.

## ACKNOWLEDGMENTS

The authors acknowledge Jan Gärtner for his help in the AFM measurement.

## REFERENCES

(1) Schenk, T.; Pešić, M.; Slesazeck, S.; Schroeder, U.; Mikolajick, T. Memory technology—a primer for material scientists. *Rep. Prog. Phys.* **2020**, *83*, 086501.

(2) Schenk, T.; Mueller, S. A New Generation of Memory Devices Enabled by Ferroelectric Hafnia and Zirconia. *IEEE International Symposium on Applications of Ferroelectrics (ISAF)*, 2021; pp 1−11.

(3) Pešić, M.; Schroeder, U.; Mikolajick, T. Ferroelectric One Transistor/One Capacitor Memory Cell. *Ferroelectricity in Doped Hafnium Oxide: Materials, Properties and Devices*; Elsevier, 2019; pp 413−424.

(4) Luo, Q.; Cheng, Y.; Yang, J.; Cao, R.; Ma, H.; Yang, Y.; Huang, R.; Wei, W.; Zheng, Y.; Gong, T.; Yu, J.; Xu, X.; Yuan, P.; Li, X.; Tai, L.; Yu, H.; Shang, D.; Liu, Q.; Yu, B.; Ren, Q.; Lv, H.; Liu, M. A highly CMOS compatible hafnia-based ferroelectric diode. *Nat. Commun.* **2020**, *11*, 1391.

(5) Francois, T.; Pellissier, L.; Slesazeck, J.; Havel, P.; Richter, C.; Makosiej, N.; Giraud, T.; Breyer, F.; Materano, V.; Chiquet, C.; Bocquet, S.; Grenouillet, V.; Nowak, C.; Schroeder, A.; Gaillard, B.; Coignus, E. T.; Blaise, M.; Carabasse, P.; Vaxelaire, M.; Magis, E.; Aussenac, U.; Loup, F. Demonstration of BEOL-compatible ferroelectric $Hf_{0.5}Zr_{0.5}O_2$ scaled FeRAM co-integrated with 130 nm CMOS for embedded NVM applications. *IEEE International Electron Devices Meeting (IEDM)*, 2019; pp 15.7.1−15.7.4.

(6) Kim, S. J.; Narayan, D.; Lee, J.; Mohan, J.; Lee, J. S.; Lee, J.; Kim, H. S.; Byun, Y.; Lucero, A. T.; Young, C. D.; Summerfelt, S. R.; San, T.; Colombo, L.; Kim, J. Large ferroelectric polarization of TiN/$Hf_{0.5}Zr_{0.5}O_2$/TiN capacitors due to stress-induced crystallization at low thermal budget. *Appl. Phys. Lett.* **2017**, *111*, 242901.

(7) Lehninger, D.; Olivo, R.; Ali, T.; Lederer, T.; Kämpfe, C.; Mart, K.; Biedermann, K.; Kühnel, L.; Roy, M.; Kalkani, K.; Seidel, K. Back-End-of-Line Compatible Low-Temperature Furnace Anneal for Ferroelectric Hafnium Zirconium Oxide Formation. *Phys. Status Solidi A* **2020**, *217*, 1900840.

(8) Kim, H. J.; An, Y.; Jung, Y.; Mohan, J.; Yoo, J.; Kim, Y.; Hernandez-Arriaga, H.; Kim, H.; Kim, J.; Kim, S. Low-Thermal-Budget Fluorite-Structure Ferroelectrics for Future Electronic Device Applications. *Phys. Status Solidi RRL* **2021**, *15*, 2100028.

(9) Böscke, T. S.; Müller, J.; Bräuhaus, D.; Schröder, U.; Böttger, U. Ferroelectricity in hafnium oxide thin films. *Appl. Phys. Lett.* **2011**, *99*, 102903.

(10) Xu, L.; Nishimura, T.; Shibayama, S.; Yajima, T.; Migita, S.; Toriumi, A. Kinetic pathway of the ferroelectric phase formation in doped $HfO_2$ films. *J. Appl. Phys.* **2017**, *122*, 124104.

(11) Mittmann, T.; Materano, M.; Lomenzo, P. D.; Park, M.; Stolichnov, I.; Cavalieri, M.; Zhou, C.; Chung, C.; Jones, J. L.; Szyjka, T.; Müller, M.; Kersch, A.; Mikolajick, T.; Schroeder, U. Origin of Ferroelectric Phase in Undoped $HfO_2$ Films Deposited by Sputtering. *Adv. Mater. Interfac.* **2019**, *6*, 1900042.

(12) Bouaziz, J.; Romeo, P. R.; Baboux, N.; Vilquin, B. Huge Reduction of the Wake-Up Effect in Ferroelectric HZO Thin Films. *ACS Appl. Electron. Mater.* **2019**, *1*, 1740−1745.

(13) Luo, Q.; Ma, H.; Su, H.; Xue, K.; Cao, R.; Gao, Z.; Yu, J.; Gong, T.; Xu, X.; Yin, J.; Yuan, P.; Tai, L.; Dong, D.; Long, S.; Liu, Q.; Miao, X.; Lv, H.; Liu, M. Composition-Dependent Ferroelectric

Properties in Sputtered $Hf_{X}Zr_{1-X}O_2$ Thin Films. *IEEE Electron Device Lett.* **2019**, *40*, 570−573.
(14) Hsain, H. A.; Lee, Y.; Materano, M.; Mittmann, T.; Payne, A.; Mikolajick, T.; Schroeder, U.; Parsons, G. N.; Jones, J. L. Many routes to ferroelectric $HfO_2$ : A review of current deposition methods. *J. Vac. Sci. Technol., A* **2022**, *40*, 010803.
(15) Wang, X.; Mikolajick, T.; Grube, M. Assessment of Back-End-of-Line Compatibility of Sputtered $HfO_2$ -Based Ferroelectrics. *Phys. Status Solidi - Rapid Res. Lett.* **2022**, *16*, 2100572.
(16) Institute of Electrical and Electronics Engineers. International Roadmap for Devices and Systems (IRDS). IEEE 2021. [Online]. Available: https://irds.ieee.org/editions/2021 (accessed Nov 07, 2022)
(17) Gates-Rector, S.; Blanton, T. The Powder Diffraction File: a quality materials characterization database. *Powder Diffr.* **2019**, *34*, 352−360.
(18) Materano, M.; Richter, C.; Mikolajick, T.; Schroeder, U. $Hf_{x}Zr_{1-x}O_2$ thin films for semiconductor applications: An Hf- and Zr-ALD precursor comparison. *J. Vac. Sci. Technol., A* **2020**, *38*, 022402.
(19) Lee, Y. H.; Kim, H.; Moon, T.; Kim, K.; Hyun, S.; Park, H.; Lee, Y.; Park, M.; Hwang, C. Preparation and characterization of ferroelectric $Hf_{0.5}Zr_{0.5}O_2$ thin films grown by reactive sputtering. *Nanotechnology* **2017**, *28*, 305703.
(20) Gao, P.; Meng, L. J.; dos Santos, M. P.; Teixeira, V.; Andritschky, M. Influence of sputtering pressure on the structure and properties of ZrO2 films prepared by rf reactive sputtering. *Appl. Surf. Sci.* **2001**, *173*, 84−90.
(21) Dave, V.; Dubey, P.; Gupta, H. O.; Chandra, R. Influence of sputtering pressure on the structural, optical and hydrophobic properties of sputtered deposited HfO2 coatings. *Thin Solid Films* **2013**, *549*, 2−7.
(22) Sharma, G.; Ushakov, S. V.; Navrotsky, A. Size driven thermodynamic crossovers in phase stability in zirconia and hafnia. *J. Am. Ceram. Soc.* **2018**, *101*, 31−35.
(23) Behrisch, R.; Eckstein, W. *Sputtering by Particle Bombardment: Experiments and Computer Calculations from Threshold to MeV Energies*; Springer, 2007.
(24) Ono, T.; Kenmotsu, T.; Muramoto, T. Simulation of the Sputtering Process. In *Reactive Sputter Deposition. 109*; Depla, D., Mahieu, S., Eds.; Springer, 2008; pp 1−42.
(25) Hoffmann, M.; Schroeder, U.; Schenk, T.; Shimizu, T.; Funakubo, H.; Sakata, O.; Pohl, D.; Drescher, M.; Adelmann, C.; Materlik, R.; Kersch, A.; Mikolajick, T. Stabilizing the ferroelectric phase in doped hafnium oxide. *J. Appl. Phys.* **2015**, *118*, 072006.
(26) Lederer, M.; Lehninger, D.; Ali, T.; Kämpfe, T. Review on the Microstructure of Ferroelectric Hafnium Oxides. *Phys. Status Solidi - Rapid Res. Lett.* **2022**, *16*, 2200168.
(27) Schroeder, U.; Park, M. H.; Mikolajick, T.; Hwang, C. S. The fundamentals and applications of ferroelectric HfO2. *Nat. Rev. Mater.* **2022**, *7*, 653−669.
(28) Park, M. H.; Lee, Y. H.; Mikolajick, T.; Schroeder, U.; Hwang, C. S. Review and perspective on ferroelectric HfO2-based thin films for memory applications. *MRS Commun.* **2018**, *8*, 795−808.
(29) Mueller, S.; Muller, J.; Schroeder, U.; Mikolajick, T. Reliability Characteristics of Ferroelectric Si:$HfO_2$ Thin Films for Memory Applications. *IEEE Trans. Device Mater. Reliab.* **2013**, *13*, 93−97.
(30) Bouaziz, J.; Rojo Romeo, P.; Baboux, N.; Negrea, R.; Pintilie, L.; Vilquin, B. Dramatic impact of pressure and annealing temperature on the properties of sputtered ferroelectric HZO layers. *APL Mater.* **2019**, *7*, 081109.
(31) Hara, Y.; Mohit; Murakami, T.; Migita, S.; Ota, H.; Morita, Y.; Tokumitsu, E. Impact of reduced pressure crystallization on ferroelectric properties in hafnium-zirconium dioxide films deposited by sputtering. *Jpn. J. Appl. Phys.* **2021**, *60*, SFFB05.
(32) Shibayama, S.; Nishimura, T.; Migita, S.; Toriumi, A. Thermodynamic control of ferroelectric-phase formation in $Hf_{x}Zr_{1-x}O_2$ and $ZrO_2$. *J. Appl. Phys.* **2018**, *124*, 184101.
(33) Migita, S.; Ota, H.; Asanuma, S.; Morita, Y.; Toriumi, A. Accelerated ferroelectric phase transformation in $HfO_2$ /$ZrO_2$ nanolaminates. *Appl. Phys. Express* **2021**, *14*, 051006.
(34) Woo, J.; Goh, Y.; Im, S.; Hwang, J.; Kim, Y.; Kim, J.; Im, J.; Yoon, S.; Moon, S.; Jeon, S. Improved Ferroelectric Switching in Sputtered $HfZrO_x$ Device Enabled by High Pressure Annealing. *IEEE Electron Device Lett.* **2019**, *41*, 232−235.
(35) Alcala, R.; Materano, M.; Lomenzo, P. D.; Grenouillet, L.; Francois, T.; Coignus, J.; Vaxelaire, N.; Carabasse, C.; Chevalliez, S.; Andrieu, F.; Mikolajick, T.; Schroeder, U. BEOL Integrated Ferroelectric HfO2 based Capacitors for FeRAM: Extrapolation of Reliability Performance to Use Conditions. *IEEE J. Electron Devices Soc.* **2022**, *10*, 907.
(36) Kim, S. J.; Jung, Y.; Mohan, J.; Kim, H.; Rho, S.; Kim, M.; Yoo, J.; Park, H.; Hernandez-Arriaga, H.; Kim, J.; Kim, H.; Choi, D.; Jung, J.; Hwang, S.; Sejoon Kim, H.; Kim, H.; Kim, J. Low-thermal-budget (300 °C) ferroelectric TiN/$Hf_{0.5}Zr_{0.5}O_2$ /TiN capacitors realized using high-pressure annealing. *Appl. Phys. Lett.* **2021**, *119*, 242901.




https://doi.org/10.1021/acsaelm.2c01259
ACS Appl. Electron. Mater. 2022, 4, 6142−6148

# Supporting Information

## Sputtered Ferroelectric Hafnium-Zirconium Oxide with High Remanent Polarization after Back-End-of-Line Compatible Annealing

Xuetao Wang[1, *], Thomas Mikolajick[1, 2], Matthias Grube[1, *]

[1]*NaMLab gGmbH, Nöthnitzer Str. 64a, Dresden 01187, Germany*

[2]*Chair of Nanoelectronics, TU Dresden, Nöthnitzer Str. 64, Dresden 01187, Germany*

*Corresponding: Xuetao.Wang@namlab.com; Matthias.Grube@namlab.com*

## Deposition rate of the HZO films

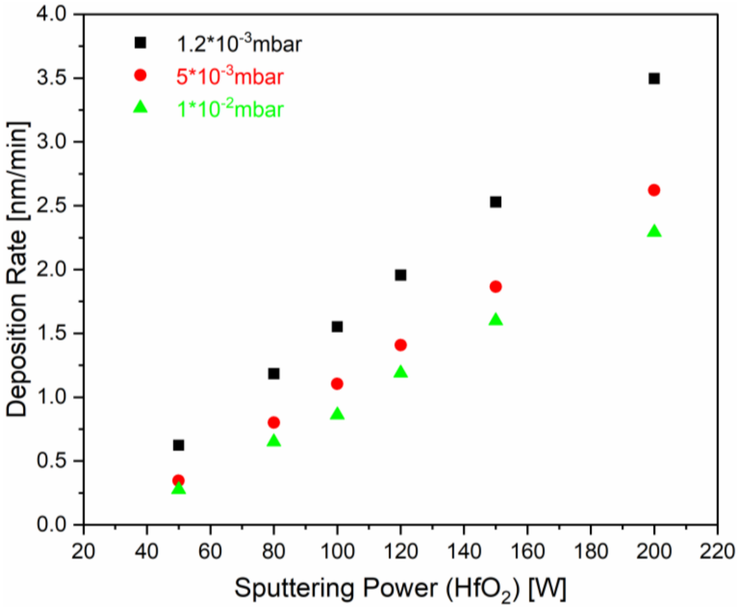


**Figure S1**. Deposition rate of the HZO (87:13) films at different sputtering pressure as a function of the sputtering power.

The overall sputtering power for $HfO_2$ and $ZrO_2$ targets was not the same for different pressures if a constant concentration is targeted, which is 13 % $ZrO_2$ in this work. Hence, the sputtering power for $HfO_2$ is used to represent the samples with varying sputter power in **Figure S1**.

## Surface chemical composition of the HZO samples by X-ray photoelectron spectroscopy

**Table S1**. Surface chemical composition of the hafnium-zirconium oxide calculated from the X-ray photoelectron spectroscopy spectra.

| Samples | Concentration (at. %) | | | | | | Concentration ratio | |
|---|---|---|---|---|---|---|---|---|
| | C | O (organics) | O (oxide) | Hf | Zr | Ti | Hf:Zr | (Hf+Zr+Ti):O |
| 100W:50W | 22.4 | 14.9 | 41.4 | 18.1 | 2.8 | 0.5 | 87:13 | 1:1 |
| 150W:67W | 19.3 | 11.1 | 46.8 | 19.0 | 3.0 | 0.9 | 87:13 | 1:1 |

In **Table S1**, two samples' hafnium-zirconium oxides (HZO) were processed at sputtering pressure of $1.2*10^{-3}$ mbar. The sample name is abbreviated as sputtering power for $HfO_2$: sputtering power for $ZrO_2$. Therefore, the 100W:50W sample means that the ferroelectric layer was sputtered with the power of 100W on the $HfO_2$ target and 50W on the $ZrO_2$ target. Before the X-ray photoelectron spectroscopy, the TiN/HZO/TiN capacitor stack was prepared, and then TiN top electrode was etched away. As can be seen in **Table S1**, the ratio of Hf to Zr is 87:13 for both samples, proving the stoichiometry of HZO (87:13). Additionally, Ti signal was still detected from the surface of the sample, which could be from the $TiO_x$ that formed at the interface between TiN and HZO during the TiN top electrode sputtering. With the etching process used in this work, the etchant could not remove the $TiO_x$ as fast as it removed the TiN film.

**AFM height profiles along horizontal line of the samples**

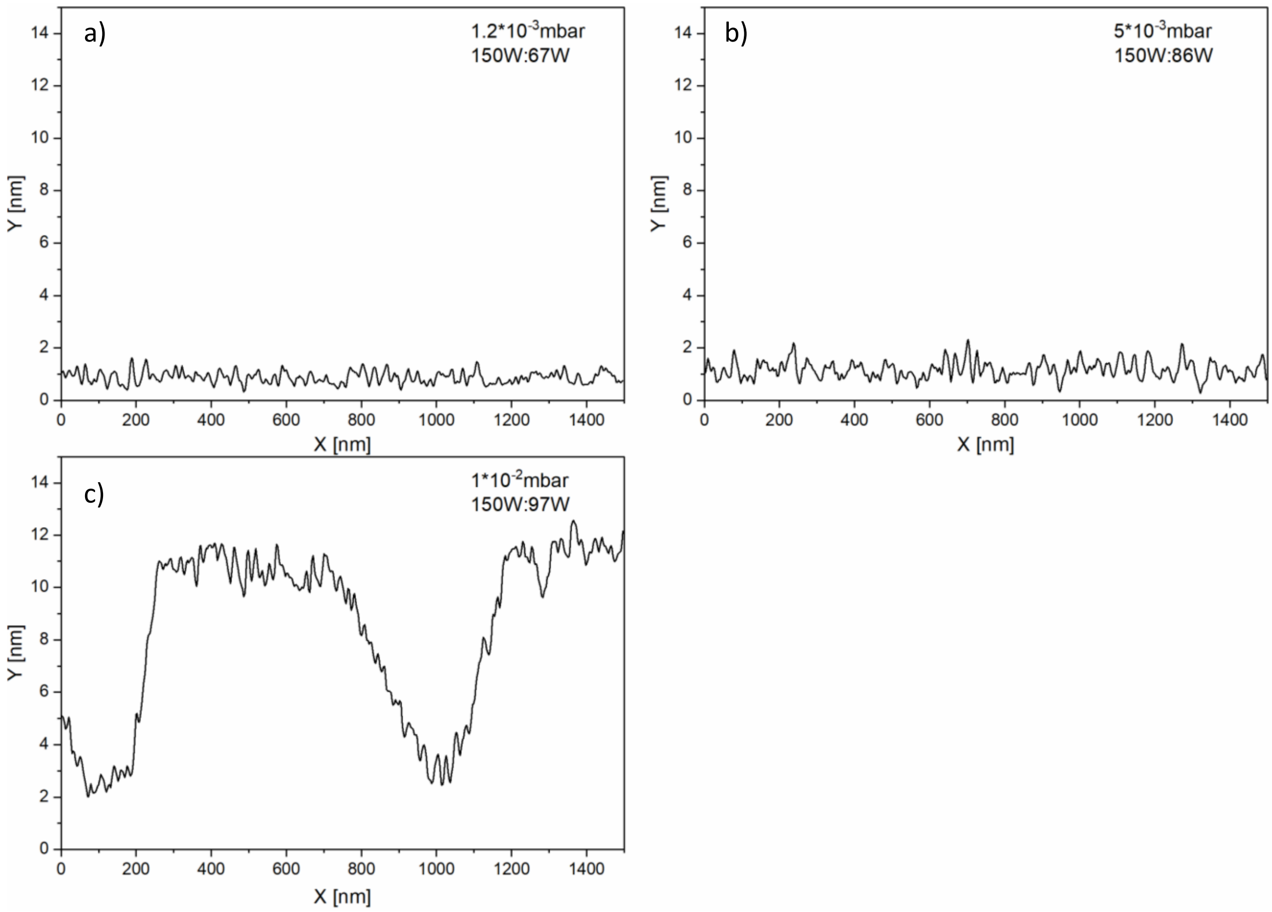


**Figure S2**. AFM height profiles along horizontal line of sputtered HZO (87:13) with different sputtering pressure and power in an FeCap stack after 800 °C annealing. The abbreviation "xxW:yyW" indicates the used powers for the $HfO_2$ and $ZrO_2$ target respectively. a) 150W:67W at $1.2*10^{-3}$ mbar (TiN top electrode etched); b) 150W:86W at $5*10^{-3}$ mbar (TiN top electrode etched); c) 150W:97W at $1*10^{-2}$ mbar (TiN top electrode etched).

The height profiles (**Figure S2**) add additional information to the AFM z-scale images as shown in **Figure 1**. Maximumly one nanometer variation in height can be seen for the $1.2*10^{-}$

[3] mbar and 5*10$^{-3}$ mbar samples, indicating smooth surfaces on those two samples. While on the 1*10$^{-2}$ mbar sample, around 10 nm thick trenches clearly exist in the HZO film.

**GIXRD of the 5*10$^{-3}$mbar samples**

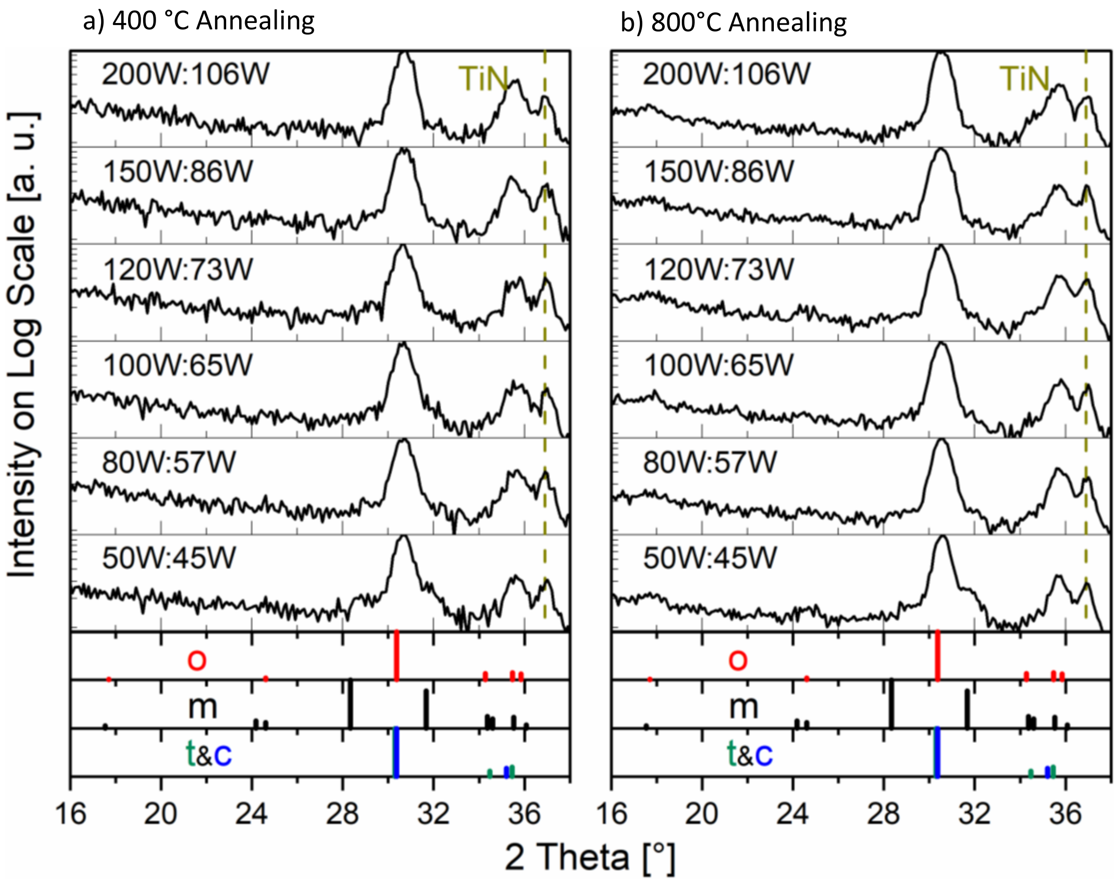


**Figure S3**. GIXRD patterns of sputtered HZO (87:13) with different sputtering power in an FeCap stack after annealing. The bar charts of a) to b) represent the different $HfO_2$ crystal phases retrieved from the ICCD database [1]. The y-axis scale (intensity) is the same for all GIXRD patterns. The abbreviation "xxW:yyW" indicates the used powers for the $HfO_2$ and $ZrO_2$ target respectively. Stack annealed at a) 400 °C; b) 800 °C.

**Endurance measurement of the 5*10$^{-3}$mbar samples**

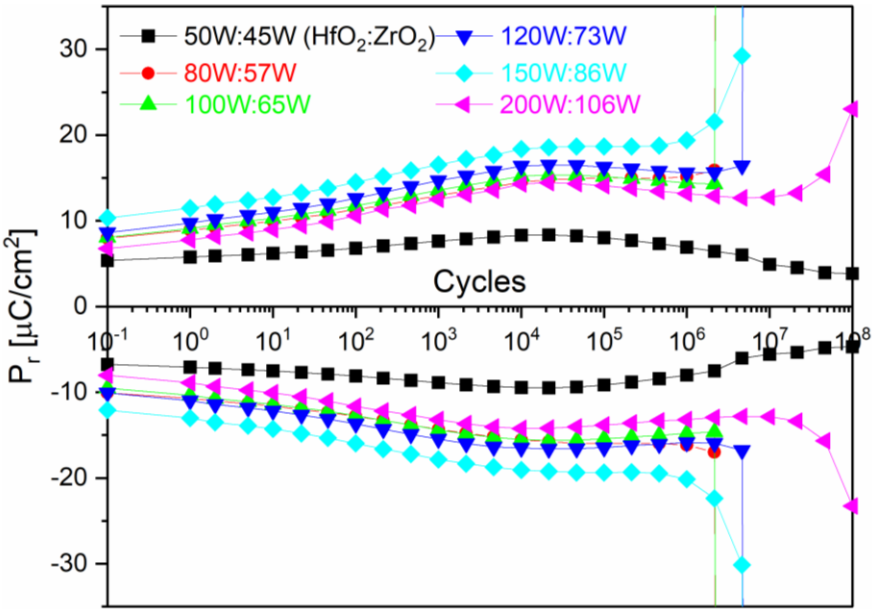


**Figure S4**. Endurance measurement of the FeCaps with the HZO (87:13) sputtered at 5*$10^{-3}$ mbar. The sputtering powers shown in the legend are for $HfO_2$ and $ZrO_2$ targets, respectively.

The typical $HfO_2$-base FE cycling behavior can be witnessed in **Figure S4**, which comprises wakeup, plateau, fatigue and breakdown. The sample with 50W:45W demonstrates a lower $P_r$, compared to other samples. This can be attributed to containing more m-phase in the HZO films, which can be seen in the GIXRD results (**Figure S3**).

REFERENCES

[1] Gates-Rector, S.; Blanton, T. The Powder Diffraction File: a quality materials characterization database. *Powder Diffr.* **2019**, 34(4), 352–360. doi: 10.1017/S0885715619000812.